20th European Symposium on Computer Aided Process Engineering – ESCAPE20
S. Pierucci and G. Buzzi Ferraris (Editors)

Optimal control solutions for crystal shape manipulation

Naim Bajcinca[a], Vinicius de Oliveira[a], Christian Borchert[a], Jörg Raisch[a,b]
Kai Sundmacher[a,c]

[a]*Max-Planck Institute for Dynamics of Complex Technical Systems, Sandtorstr.1, 39106 Magdeburg, Germany*
[b]*Technische Universität Berlin, Einsteinufer 17, 10857 Berlin, Germany*
[c]*Otto-von-Guericke Universität Magdeburg, Universitätsplatz 2, 39106 Magdeburg, Germany*

Abstract

Optimal control algorithms and strategies for crystal shape manipulation are explored in this paper. We focus on minimum time trajectories with the temperature as the control input. A challenge results from the inherent constraints in the particle growth vector, which is confined to lie within a cone in the model state-space. As a consequence, switching trajectories with a number of subsequent growth and dissolution phases may be indispensable. Such a strategy employs the unequal growth and dissolution rates in order to achieve crystal morphologies which do not result directly from a pure growth process only. For instantaneous switching between subsequent phases we need to extend the temperature solution profiles to piecewise-continuous. By a suitable specification of the switching manifolds, we are then able to avoid unnecessary long paths in the state-space. Diverse solution approaches to the optimal control problem are suggested using the minimum principle and efficient numerical techniques which utilize the invertibility property of the particle growth dynamics. In particular, we prove that minimum-time scenarios are composed of constant supersaturation trajectory sections.

Keywords: Crystal shape manipulation, optimal control, dynamic inversion, batch processes, multidimensional crystallization

1. Introduction & Motivation

Crystal shape is critical for sophisticated particle products in numerous industries. Properties of dispersed phase products are strongly linked to their shape. For instance, the surface structure and binding energies, and thus reactivity, varies with crystallographic orientation [10]. From the engineering point of view, manipulation of the crystal morphology is therefore essential. While much of the effort in the past has gone into the control and optimization of 1-D crystal-size-distributions [2,4], research on multidimensional crystallization processes has been scarce despite of its evident importance in practice. The limitations in monitoring of crystal shape has been recognized as the major bottleneck [1]. As a consequence, traditional approaches in crystal shape manipulation, as applied in industrial processes like crystallization or precipitation, shifted towards purely chemical techniques. For instance, utilization of additives (see [9]) for blocking or promoting of certain crystal faces has been widely used, despite the fact that, thereby, chemical impurities may arise. However, recent progress in image processing techniques for particle shape monitoring has been an impetus for intensification of theoretical research efforts in modeling and control of multidimensional crystallization processes. In this paper, optimization algorithms for crystal shape manipulation by temperature control only are proposed, by making use of the measurement of concentration and online monitoring of the crystal particle shape.

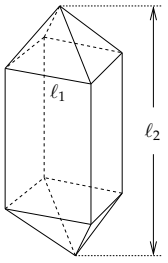

Figure 1: KDP

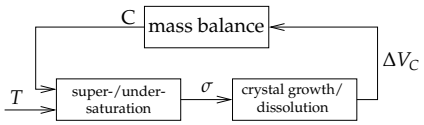

Figure 2: Batch feedback loop

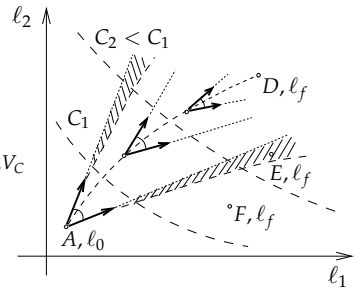

Figure 3: Reachability regions

2. Particle shape dynamics

Crystal particle shape dynamics is modeled as a negative feedback structure, as shown in Figure 2. Any temperature (T) change affects supersaturation σ, which in turn forces the crystal to grow or dissolve in order to retain the mass balance equilibrium. The corresponding equations are standard, *e.g.,* see [7],

$$\text{particle growth: } \mathrm{d}\ell_i/\mathrm{d}t = k_{g_i}\sigma^{g_i} \triangleq G_i, \text{ with } \sigma \geq 0 \text{ and } i = 1,2,\cdots,n \tag{1}$$

$$\text{particle dissolution: } \mathrm{d}\ell_i/\mathrm{d}t = -k_{d_i}(-\sigma)^{d_i} \triangleq G_i, \text{ with } \sigma \leq 0 \text{ and } i = 1,2,\cdots,n \tag{2}$$

$$\text{supersaturation: } \sigma = C/C_{\text{sat}} - 1,\ C_{\text{sat}} = a_0 + a_1 T + a_2 T^2,\ a_i > 0,\ i = 0,1,2 \tag{3}$$

$$\text{mass balance: } C = C_0 - \rho_C/V_t M \cdot \Delta V_C,\ V_C = V_C(\ell_1, \ell_2, \cdots, \ell_n) \tag{4}$$

where C stands for the concentration, C_{sat} for saturation concentration, $\Delta V_C = V_C - V_{C,0}$ for crystal volume change, $V_{C,0}$ for the initial crystal volume, ρ_C for crystal mass density, M for solvent molar mass, and V_t for the solvent volume. As case study we consider the two-dimensional potassium dihydrogen phosphate (KH_2PO_4, abbr. KDP) particle, see Figure 1. The numerical data are taken from [5].

The model setting as suggested in (1)-(4) is simplifying for a number of reasons. The growth rate coefficients in different dimensions are assumed to be independent in (1), though experimental reports on coupled growth rate kinetics exist. Nucleation is neglected, but this simplification will not contest our key results. Furthermore, we consider here a single particle only, not a population distribution.

Figure 3 provides a qualitative reachability analysis for trajectories starting at an arbitrary point A in the ℓ-space ($\mathbb{R}^n_+$) for $n = 2$. The growth rate vector $G = \mathrm{d}\ell/\mathrm{d}t$, as defined in (1)-(4), is constrained to lie within a cone parameterized by the supersaturation level σ lying between a minimal value $\sigma_{\min}$ corresponding due to the maximal temperature $T_{\max}$, and a maximal value $\sigma_{\max}$ corresponding to the minimal temperature $T_{\min}$. Obviously, as the particle grows, the supersaturation σ decreases, while the growth cone narrows and rotates clock-wise (for $g_2 > g_1$). In Figure 3, a reachable (dashed) region below the cone with the apex at A appears, while an upper (dashed) piece is lost. This delineated reachability picture is further affirmed by the decrease in the concentration due to the nucleation phenomenon. In this paper, we primarily address (but not confine to) the *reachable* targets within the constraint cone at the starting point A (*e.g., D*). All such points are connected by a straight line segment. Such trajectories are particularly important in this study.

For $\Delta V_c \rho_C \ll V_t M$ the concentration C remains nearly constant, $C \approx C_0$, and the mass balance feedback decouples in Figure 2. In the next section, this particularly simple situation is examined to gain insight into the optimal solutions in the general case.

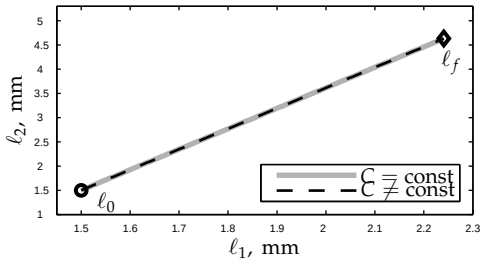

Figure 4: Path profile

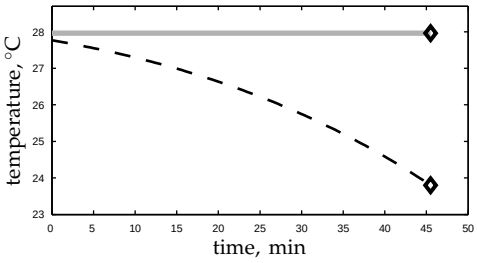

Figure 5: Temperature profile

3. Optimal control algorithms

3.1. A single growth trajectory

Consider a two-dimensional particle and let $C = C_0 = const$. We construct first the minimum-time trajectory starting from $\ell_0 = \ell(0)$ for a reachable target $\ell_f = \ell(t_f)$ within its growth constraint cone. According to the Pontryagin's minimum principle (see *e.g.,* [8]), we seek for the optimal inputs $u = u^*$ which minimize the Hamiltonian H defined by

$$H(u,p) = 1 + p^T G(u), \tag{5}$$

where $p = [p_1, p_2]^T$ is the costate vector, and $G = [G_1, G_2]^T$. Note that instead of T, we can equivalently set $u = \sigma = C_0/C_{\text{sat}} - 1$ as the independent input. The costates evolve as $\dot{p}_1 = -\partial H/\partial \ell_1 = 0$ and $\dot{p}_2 = -\partial H/\partial \ell_2 = 0$, i.e. they are constant, $p_1 = p_1^*$ and $p_2 = p_2^*$. Hence, H is a function of σ only, and, the optimal $u^* = \sigma^*$ is obtained from $\partial H/\partial u = 0$

$$\sigma^* = (-p_1^* k_{g_1} g_1 / p_2^* k_{g_2} g_2)^{\frac{1}{g_2 - g_1}}. \tag{6}$$

The costates $p_1 = p_1^*$ and $p_2 = p_2^*$, as well as, $t_f = t_f^*$, are obtained as solutions to the boundary value problem

$$\ell_f = G(\sigma^*) \cdot t_f^* + \ell_0, \;\; H(\sigma^*, p^*) = 0. \tag{7}$$

To summarize, the solution to the minimum-time problem is a linear trajectory driven by a *constant supersaturation* $\sigma^* = const$. Note that σ^* computed from (6) must be feasible ($\sigma_{\min} < \sigma^* < \sigma_{\max}$), since there is a unique line segment which connects ℓ_0 and ℓ_f. The corresponding optimal temperature $T^* = const$ is also constant and it can be analytically computed from (6) and (3).

The equations (6) and (7) hold even if the assumption $C = const$ is dropped. Indeed, we only need to readjust the temperature profile to fulfill the mass balance equation (4) by solving the equation

$$C_{\text{sat}}(T^*) = C(\ell)/(1 + \sigma^*), \tag{8}$$

where σ^* is from (6) and $\ell = \ell(t)$. Numerical results for our case-study are shown in Figure 4 and 5. The plots in gray refer to the simplified case $C = C_0 = const$, and the dashed ones to the complete model. Notice that, in both cases, the optimal trajectory is linear, indicating a constant supersaturation level. The concentration $C = C(\ell)$ is now effected by the mass balance, but the temperature decreases in order to keep the supersaturation at the constant level σ^*. The two optimal solutions provide the identical optimized value for the process duration $t_f^* \approx 45$ [min], see Figure 5.

The extension of the minimum principle approach to the case with an n-dimensional particle is rather straightforward. The boundary value problem (7) provides now $n+1$ conditions for the n unknown costates p_i, $i = 1, \cdots, n$ and the time duration t_f. To keep things simple, again (as in the two-dimensional case), any two state equations from (7) are sufficient to solve for the optimal σ^* and t_f^*. The remaining $n-2$ states affect the temperature profile via (8).

3.2. Switching trajectories

Target points, such as F in Figure 3, are not reachable from A without further ado. One is forced to switch at some point from the growth to a dissolution mode, see [3]. In this section, we provide conditions for minimum-time trajectories comprising a fixed number of switching phases. As switching manifolds we specify the manifolds in $\ell-$space corresponding to a constant concentration or (according to (4)), equivalently, to a constant particle volume

$$\text{growth to dissolution: } m_u(\ell) = V_C(\ell) - V_u = 0, \;\; V_u \text{ fixed} \tag{9}$$

$$\text{dissolution to growth: } m_l(\ell) = V_C(\ell) - V_l = 0, \;\; V_l \text{ fixed} \tag{10}$$

For simplicity, consider a single-switching trajectory. Let t_b be the switching time instant from a growth to a dissolution mode. Then the Hamiltonian function reads

$$H = 1 + p_+^T G_+ \triangleq H_+, \; 0 < t < t_b, \;\text{ and }\; H = 1 + p_-^T G_- \triangleq H_-, \; t_b < t < t_f. \tag{11}$$

where the subscript "$+$" refers to the growth and "$-$" to the dissolution mode. Using the arguments of the previous section we know that the costates p_+ and p_- must remain constant within a switching mode. In accordance with the minimum principle, the boundary value problem now extends to

$$\text{growth mode: } \ell_b = G_+ \cdot t_b + \ell_0, \;\; m_u(l_b) = 0 \tag{12}$$

$$\text{switching conditions: } H_+(t_b) = H_-(t_b), \;\; p_+ = p_- + \lambda \cdot \partial m_u / \partial \ell|_{\ell_b} \tag{13}$$

$$\text{dissolution mode: } \ell_f = G_- \cdot (t_f - t_b) + \ell_b, \; H_-(t_f) = 0, \tag{14}$$

where we require continuity for the Hamiltonian at the switching time instant, and introduce a Lagrange-multiplier λ for the switching manifold $m_u(\ell) = 0$ at the switching point ℓ_b. The above system of nonlinear algebraic equations provides $3n+3$ conditions on ℓ_b, p_+, p_-, t_b, t_f and λ, i.e. on $3n+3$ unknowns. Notice that, due to the continuity of the Hamiltonian, the costates must jump from p_+ to p_- at the switching moment. Again, the minimum-time single-switching trajectory consists of two linear trajectory sections with *constant supersaturation levels*. At the switching point the optimal value of supersaturation jumps from $\sigma_+^* > 0$ to $\sigma_-^* < 0$, which satisfy equations of the form (6). In other words, the optimal control policy imposes a *discontinuity* in the optimal temperature profile.

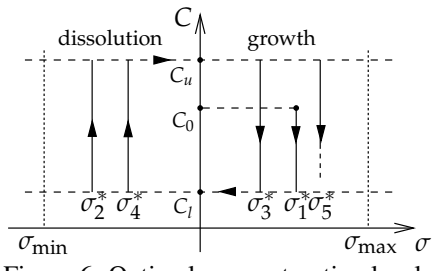

Figure 6: Optimal supersaturation levels

The optimal switching conditions (12)-(14) are easily generalized for a multiple switching trajectory. Figure 6 illustrates a switching control policy between optimal supersaturation levels in the $(\sigma - C)$-plane. The number of unknown variables and conditions of the boundary value problem increases by $2n+2$ with each additional switching. In total, a trajectory including η switching modes, involves a system of $(2\eta+1)(n+1)$ nonlinear algebraic equations.

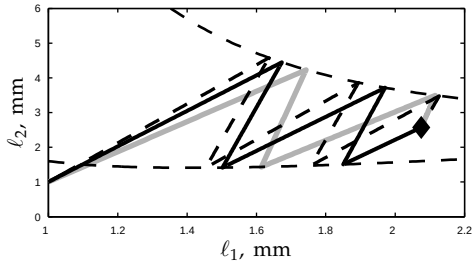

Figure 7: Path profile

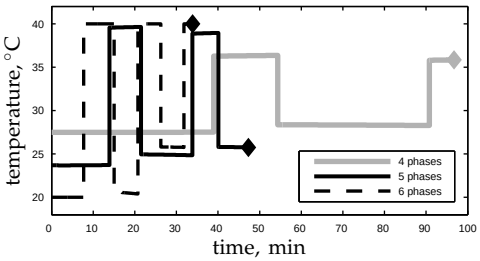

Figure 8: Temperature profile

3.3. Numerical optimization algorithms

For a trajectory involving η switchings we expect from an optimization algorithm to decide on $\eta+1$ constant optimal supersaturation levels σ_i^*, $i=1,\cdots,\eta+1$, see Figure 6. Using the facts from Section 3.2, we formulate the following nonlinear programming problem in terms of the decision variables σ_i and $\ell_1^{(i)}$

$$\begin{gathered}\min \textstyle\sum_{i=1}^{\eta+1} \frac{\Delta\ell_1^{(i)}}{G_1(\sigma_i)} \\ \text{s.t. } m_u(\ell^{(i)})=0, 0\le\sigma_i\le\sigma_{\max}, i\in\mathbb{N}_{\text{o}}, m_l(\ell^{(i)})=0, \sigma_{\min}\le\sigma_i\le 0, i\in\mathbb{N}_{\text{e}} \\ \text{where } \Delta\ell_1^{(i)}=\ell_1^{(i)}-\ell_1^{(i-1)},\ \ell^{(i)}=\frac{G(\sigma_i)}{G_1(\sigma_i)}\Delta\ell_1^{(i)}+\ell^{(i-1)},\ \ell^{(0)}=\ell_0,\ \ell^{(\eta+1)}=\ell_f,\end{gathered} \tag{15}$$

where the symbol $\ell^{(i)}$ stands for the i^{th} switching point on the manifolds $m_u(\ell)$ (if i is even) or $m_l(\ell)$ (if i is odd). Note that the i^{th} summing term in the cost function represents the time length of the i^{th} switching phase. Without loss of generality, we start here with a growth phase. The decision variables $\ell_1^{(i)}$ and σ_i count up to $2\eta+1$. The number of variables which the optimizer in (15) has to decide on reduces to $1/(n+1)^{\text{th}}$ as compared to the boundary value problem in the previous section.

Obviously, the problem formulation (15) applies for trajectories consisting of linear sections only. For "non-linearly" reachable targets, such as E in the dashed region in Figure 3, the profiles provided by (6) are not feasible. Therefore, we propose a numerical algorithm, which makes use of the invertible structure of the model (1)-(4). Indeed, given the functions $\ell_1=\ell_1(t)$ and $G_1=\mathrm{d}\ell_1/\mathrm{d}t$, all the system variables, *i.e.* $\ell(t)=[\ell_1(t),\ell_2(t),\cdots,\ell_n(t)]^T$, $\sigma(t)$ and $T(t)$, are uniquely determined as follows

$$\sigma(t)=(G_1/k_{g1})^{\frac{1}{g_1}},\ \ \ell_i(t)=\int k_{gi}\sigma^{g_i}\mathrm{d}t,\ \ C_{\text{sat}}(T)=C(\ell)/(1+\sigma). \tag{16}$$

Now, introduce a parametrization $\ell_1(t)=\ell_{1,0}+\alpha^T\psi(t)$, where α^T is a parameter vector and $\psi(t)$ includes functions from a convenient basis (*e.g.,* B-splines). It is important to note that $\ell_i(t)$ in (16) are integrable in closed form, i.e. the expression $\ell(t)=\ell(\alpha,\psi(t))$ is analytically available. The dynamic optimization problem reduces again to a nonlinear program with α as the decision variable

$$\min t_f(\alpha^*)\ \text{ s.t. } \ell_0+\ell(\alpha^*,\psi(t_f))=\ell_f,\ k_{g1}\sigma_{\min}^{g_1}\le G_1(\alpha^*,\psi(t))\le k_{g1}\sigma_{\max}^{g_1}. \tag{17}$$

The notation $t_f(\alpha^*)$ indicates that t_f can be computed from $\ell_{1,0}+\alpha^{*T}\psi(t_f)=\ell_{1,f}$. The algorithm (17) is easily extended to switching trajectories. A switching time instant t_b can be computed by solving algebraic equations of the form $m_{u/l}(\ell(\alpha,\psi(t_b)))=0$, which apply when a trajectory section hits onto a switching manifold.

A slightly different, but a more direct trajectory parametrization, uses the fact that the whole information on a growth trajectory $\ell = \ell(t)$ is contained in its projection into any two-dimensional (*e.g.,* $(\ell_1, \ell_2)-$) plane. Indeed, then

$$\sigma(\ell_1) = \left(\frac{k_{g1}}{k_{g2}}\frac{\mathrm{d}\ell_2}{\mathrm{d}\ell_1}\right)^{\frac{1}{g_2-g_1}},\ t_f = \int_{\ell_{1,0}}^{\ell_{1,f}} \frac{\mathrm{d}\ell_1}{k_{g1}\sigma^{g_1}},\ \ell_i = \int \frac{k_{gi}}{k_{g1}}\sigma^{g_i-g_1}\mathrm{d}\ell_1,\ C_{\mathrm{sat}}(T) = C(\ell)/(1+\sigma). \tag{18}$$

One can introduce a parametrization $\ell_2 = \ell_{2,0} + \alpha^T\psi(\ell_1)$ in terms of ℓ_1 and proceed analogously to the formulation in (17). While, typically, the order of the functions $\psi(\ell_1)$ is low, the expressions $\ell_i = \ell_i(\alpha, \psi(\ell_1))$ and $t_f = t_f(\alpha, \psi(\ell_{1,f}))$, $i \geq 3$, must be computed numerically.

Figures 7 and 8 present the numerical results for the case-study with different number of switching phases. Note that the optimal t_f^* reduces as the number of switchings increases. For the indicated switching manifolds in the figure, the optimization problem is not feasible for less than four and more than six switching phases. Clearly, optimal profiles tend to a bang-bang profile with an increasing number of switchings.

4. Conclusions

Different optimization strategies for multidimensional crystal shape manipulation are proposed in this article. Optimal scenarios with subsequent growth and dissolution phases have been investigated. The class of switching trajectories driven by optimal constant supersaturation levels emerge as particularly important since they produce minimum-time trajectories and are easy to implement in practice by standard constant supersaturation control. In addition, we use the invertibility property of the crystal growth dynamics to provide two efficient numerical algorithms for the construction of nonlinear minimum-time trajectories. Such algorithms are good candidates for extension to the case of crystal population distributions. Moreover, the design of the switching manifolds could be naturally embraced in a more general optimization setting.

References

[1] D. Patience and J. Rawlings (2001): *Particle-shape monitoring and control in crystallization processes*, AIChE J., 47(9):2125-2130.
[2] R. Braatz (2002): *Advanced control of crystallization processes*, An. Rev. in Control, 26 , 87-99.
[3] R. C. Snyder, S. Studener, and M. F. Doherty (2007): *Manipulation of crystal chape by cycles of growth and dissolution*, AIChE-J., 53 (6), 1510-1517.
[4] U. Vollmer and J. Raisch (2003): *Control of batch cooling crystallisers based on orbital flatness*, Int. J. Control(1635–1643).
[5] D. L. Ma, D. K. Tafti, R. D. Braatz (2002): *High-resolution simulation of multidimensional crystal growth*, Ind. Eng. Chem. Res., 41, 6217-6223.
[6] C. Borchert, D. Ramkrishna and K. Sundmacher (2009): *Model based prediction of crystal shape distributions*, In ESCAPE19
[7] A.D. Randolph and M.A. Larson (1998): *Theory of particulate processes*, Academic Press.
[8] D.E. Kirk: *Optimal control theory: An introduction*, Dover Publications, 1998.
[9] L. Weissbuch, et al. (1995): Acta Cryst. B, 51, 115-148.
[10] H.G. Yang, et al. (2008): Nature, 453, 638-641.